An Event Based Representation for Oil Reservoir Simulation using Preconceptual Schemas.

Steven Velásquez-Chancí[a,*], Juan M. Mejía[b], Carlos M. Zapata[c]

[a] *National University of Colombia, Medellin. Department of Computer and Decision Science.*
[b] *National University of Colombia, Medellin. Department of Processes and Energy.*
[c] *National University of Colombia, Medellin. Department of Computer and Decision Science.*

Abstract

Oil reservoir simulation is governed by mass conservation laws. In such laws, flow, accumulation, sources and sinks phenomena in porous media are described. Multiple proposals for frameworks and simulations elaboration have been defined. However, those lack concepts and processes tracing, and event representation for physical phenomena. Preconceptual Schema (PS) is used for including the complete structure of an application domain and representing processes emerging in such. Cohesion, consistency, and tracing between concepts and processes is obtained by using PS. In this article, an executable model for Black oil simulation based on a preconceptual schema is proposed. The executable model is validated by running a study case. The results are in accordance with data reported in the literature. The proposed executable model allows for tracing consistently the concepts, processes, and events, which are present in Oil reservoir simulation.

Keywords: Porous Media, Executable Models, Preconceptual Schemas, Oil Reservoir Simulation, Event based Representation.

*Corresponding author
Email address: svelasquezc@unal.edu.co (Steven Velásquez-Chancí)

1. Introduction

Oil Reservoir simulation is an application of flow in porous media. Macroscopic fluid displacement through a porous rock is studied in such application. Those displacements are due to pressure, saturation, capillary and gravitational changes. Such phenomena are described by mass and momentum conservation laws, which are expressed as a coupled system of differential equations.

The black oil model (BOM) is vastly used in industrial efforts. Transport of three fluids at standard conditions is considered in this model. In addition, sink and source terms are involved, which are modeled as wells. Analytic solutions of BOM are unfeasible, hence a numerical solution is required. With this purpose, an spatial and temporal discretization is applied to BOM system of differential equations, the resulting algebraic system is solved using Newton-Raphson method.

Preconceptual schemas (PS) are intermediate representations which are useful for establishing a common point of understanding between a stakeholder and a software analyst. Furthermore, PS have elements which allow to represent both structure and dynamics of specific application domains. Moreover, Calle and Noreña **(citar)**, extended PS notation for usage in scientific software contexts, which have a greater complexity.

Mathematical models, such as BOM, are representations that appear in every effort for developing a simulator or framework for oil reservoir simulation. In addition, other representations in which, concepts and processes are shown, lack of traceability and event representation. There are proposals in which traceability is considered, but those are implementation-specific. The whole converges in oil reservoir simulators being developed in an empirical manner.

Norena, Calle and Zapata, present PS potential for representing different

application domains in scientific software contexts. In their representations, cohesion and traceability between concepts is maintained. Additionally, the whole process is traced in the elaborated PS. In this work, we present the development of an event based representation for oil reservoir simulation using Preconceptual Schemas. The developed representation consists of eight principal concepts, three events which process a simulation, and multiple functions in which reusable portions of representation are used within the PS.

Flow in porous media is an important aspect of many industrial and scientific applications. Numerical simulations of flow in porous media have been extensively done in various disciplines including oil and gas production [1], hydrology [2] and geochemical engineering [3] [4]. Accurate and efficient simulation in highly anisotropic and heterogeneous porous media remains a challenge for the traditional algorithms like finite difference method (FDM)[5], finite volume method (FVM)[6][7] or finite element method (FEM) [8] [9][10][11], due to the strong continuity required by the solution of these methods.

The methods based in conservation laws, such as FDM or FVM, have problems related to mesh degeneration, complex geometries, and when the error of the solution increases dramatically depending on mesh quality parameters [12, 13, 14]. Furthermore, these methods may not provide accurate velocity field in discontinuous and highly anisotropic media, because has to be interpolated, and this post-process introduce errors to the solution [1]. In addition, when the mesh is unstructured, the gradient reconstruction is required, not only for the velocity field calculation but also, to correct mesh deformation errors associated to skewness and non-orthogonality, increasing the overall CPU time [15] [14] [16][17].

On the other hand, methods based on the variational formulation of the

problem, such as FEM, have been regarded as a more convenient tool for numerical analysis. In addition, FEM and other methods, which can be based on variational principles or the Galerkin approach, are efficient and easily extensible for high-grade approximations replacing the traditional FDM or FVM in many applications. [8][18] [19] [20].

Recently, the Discontinuous Galerkin methods (DG) based on discontinuous approximations of the weak solutions have arisen as a good choice for solving hyperbolic systems of conservation laws. These methods have a close relationship with non-conforming FEM and work well on arbitrary meshes [21] [22]. It is important to note that DG methods do not require that the approximated solution has the same continuity of the original solution, resulting in stable high-order accurate discretizations of the diffusion operator, allowing for a simple imposition and implementation of boundary conditions and are very flexible to perform parallelization and mesh adaptivity [23]. However, despite all these advantages, the methods are not practical for real applications, especially in reservoir engineering where the simulation meshes are very large. This is due to the high computational cost, because, since there are independent basis for each element, the degrees of freedom of the method increases, increasing the memory use and the simulation time, compared to simulations with FDM, FVM or FEM schemes [24].

This work presents a method called *Hybrid Discontinuous Galerkin* (HDG), initially proposed for second order elliptic equations in [25], extended here for solving flow diffusion problems in highly anisotropic and heterogeneous porous media. Additionally HDG method has proven to be super-convergent in the isotropic case of the elliptic operator [26] and in the discretization of $p-$laplacian equation [27]. This method has a fundamental advantage the reduction of the degrees of freedom of the DG formulation, which allows a reduction in the computational cost and memory usage, compared to other classical DG methods [25]. This reduction in the degrees of freedom is due to the process of hybridiza-

tion of the trace as will be shown in the development of this work. Additionally, the presented implementation methodology allows modeling the heterogeneity in a natural way simply by assigning the respective values to the tensorial field of permeability, avoiding additional algorithms or specific implementations of interface simulation [28].

This paper is organized as follows: First, we present the governing equation of fluid flow in porous media and the mixed formulation of the problem to find not only the pressure field but also the gradient of the solution. Subsequently, we show the HDG method's formulation including some remarks about the implementation. Finally, we present three numerical examples in order to validate the method and demonstrate the efficiency and robustness of this numerical approach.

2. Mathematical Model

A model of single-phase and incompressible fluid flow through a porous media can be stated as follows: Let $\Omega \subseteq \mathbb{R}^2$ a closed domain with polygonal boundary $\Gamma := \bar{\Gamma}_D \cup \bar{\Gamma}_N$, where Γ_D and Γ_N are the Newmann and Dirichlet boundaries respectively. For a given volumetric source ($\dot{f}$), the problem is to find the pressure $P : \Omega \to \mathbb{R}$ of a fluid satisfying:

$$\begin{aligned} -\text{div}\left(\frac{\mathbb{K}}{\mu}\nabla P\right) &= \dot{f} \quad \text{in } \Omega \\ -\frac{\mathbb{K}}{\mu}\nabla P \cdot \mathbf{n} &= g_N \quad \text{on } \Gamma_N \\ P &= g_D \quad \text{on } \Gamma_D \end{aligned} \tag{1}$$

where $\mathbb{K} \in [L^\infty(\Omega)]^2$ is the permeability tensor function and $\mu \in \mathbb{R}$ the viscosity of the fluid.

2.1. Mixed formulation

To obtain the approximation of the pressure and the velocity fields, we will use a mixed formulation. This formulation will help us to find a coupled numer-

ical scheme. First, we rewrite problem (1) using the velocity field $\mathbf{U} = -\frac{\mathbb{K}}{\mu}\nabla P$ as an auxiliary variable as follows:

$$\begin{aligned} \mathbf{U} &= -\frac{\mathbb{K}}{\mu}\nabla P \quad && \text{in } \Omega \\ \text{div } \mathbf{U} &= \dot{f} && \text{in } \Omega \\ \mathbf{U}\cdot\mathbf{n} &= g_N && \text{on } \Gamma_N \\ P &= g_D && \text{on } \Gamma_D \end{aligned} \tag{2}$$

Clearly, if the problem (1) has a unique solution then the problem (2) has an unique solution without additional assumptions.

2.2. Variational formulation

Let q and $\mathbf{V}$ be scalar and vectorial functions respectively. These functions live in the same vectorial spaces of P and $\mathbf{U}$. Multiplying adequately the equations (2) by q and $\mathbf{V}$ and integrating over the domain Ω:

$$\begin{aligned} \int_\Omega \left(\frac{\mathbb{K}}{\mu}\right)^{-1} \mathbf{U}\cdot\mathbf{V} - \int_\Omega (\text{div}\mathbf{V})P + \int_\Gamma (\mathbf{V}\cdot\mathbf{n})P = 0, \\ -\int_\Omega \mathbf{U}\cdot\nabla q + \int_\Gamma (\mathbf{U}\cdot\mathbf{n})\, q = \int_\Omega \dot{f}\, q \end{aligned} \tag{3}$$

The solution $(P, \mathbf{U})$ of the strong problem (2) satisfies the integral equation (3), but this integral formulation has less regularity requests [29]. For this reason, we will focus all efforts to find a pair of functions $(\mathbf{U}_h, P_h)$ who approximate the solution of (3).

3. Methodology

The target of this paper is to approximate the solution of the pressure P and the gradient ∇P over the domain Ω as accurately as possible. For this, a discretization of the domain is needed.

3.1. Discrete formulation

Let $\mathcal{T}_h$ be a regular triangulation of $\bar{\Omega}$. The set of all edges of the triangulation is $\mathcal{E}_h$, with subsets $\mathcal{E}_I$ and $\mathcal{E}_\Gamma$ corresponding to the interior and the

boundary faces. We will find a discontinuous approximations $(\mathbf{U}_h, P_h)$ to the solution $(\mathbf{U}, P)$. Furthermore, the approximations of P and $\mathbf{U}$ over the skeleton $\mathcal{E}_h$, will be denoted $\hat{P}$ and $\hat{\mathbf{U}}$ respectively. A geometrical interpretation of these
130 *numerical fluxes* is shown in Figure 1.

The HDG formulation requires the following relation between the unknowns [30]

$$\hat{\mathbf{U}} \cdot \mathbf{n} = \mathbf{U}_h \cdot \mathbf{n} + \xi(P_h - \hat{P}) \tag{4}$$

for some positive penalty function $\xi > 0$ defined on $\partial\mathcal{T}_h := \sum_{\mathcal{E}_h} \partial K$ and constant on each face of the triangulation.

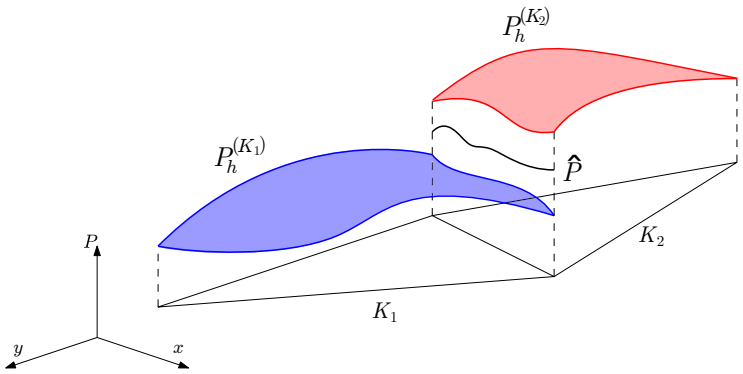

Figure 1: Geometrical interpretation of the numerical flux approximation.

Over each triangle $K \in \mathcal{T}_h$ the problem (3) can be rewritten as: *To find* $(\boldsymbol{U}_h, P_h, \hat{P})$ *such that:*

$$\begin{aligned} \int_K \left(\frac{\mathbb{K}}{\mu}\right)^{-1} \mathbf{U}_h \cdot \mathbf{V}_h - \int_K (\mathrm{div}\mathbf{V}_h) P_h &= -\int_{\partial K} (\mathbf{V}_h \cdot \mathbf{n}) \hat{P}, \\ \int_K (\mathrm{div}\mathbf{U}_h) q_h - \int_{\partial K} \xi\, P_h\, q_h &= \int_{\partial K} \xi\, \hat{P}\, q_h + \int_K \dot{f}\, q_h, \end{aligned} \tag{5}$$

with q_h and $\mathbf{V}_h$ enough regular. Summing over all faces, the normal trace must satisfy

$$\int_{\partial\mathcal{T}_h} \Big(\mathbf{U}_h \cdot \mathbf{n} + \xi(P_h - \hat{P})\Big)\, \mu = \int_{\partial\mathcal{T}_h} \tilde{g}_N \mu, \tag{6}$$

for all μ defined at $\mathcal{E}_h$ and where $\tilde{g}_N$ is the extension by zero of g_N over $\mathcal{E}_h$. The equation (6) can be called the *Continuity of the normal trace* and guarantees

the consistency of the complete scheme.

The set of equations (5) is called *Local solver*. Thereby, if we know the solution at edges, reconstruction of the solution P_h and $\mathbf{U}_h$ is straightforward.

3.2. Implementation

For each K and over the edges e in the triangulation $\mathcal{E}_h$, define the following finite dimensional approximation spaces:

$$\begin{aligned} \mathbb{P}_{r_1}(K) &= \text{span}\left(\{\psi_j\}_{j=1}^{D_1}\right), \\ [\mathbb{P}_{r_2}(K)]^2 &= \text{span}\left(\{\boldsymbol{\varphi}_j\}_{j=1}^{D_2}\right), \\ \mathbb{P}_{r_1}(e) &= \text{span}\left(\{\phi_j\}_{j=1}^{D_1-1}\right) \end{aligned} \tag{7}$$

Then we can write $\mathbf{U}_h$, P_h, $\hat{P}$ as lineal combinations of the basis functions (7). Replacing the finite projections $\mathbf{U}_h$, P_h on (5) the result is the following *local lineal system*

$$\begin{bmatrix} \mathbf{A}^K & -\mathbf{B}^K \\ \mathbf{B}^{K^T} & \mathbf{C}^K \end{bmatrix} \begin{bmatrix} [\mathbf{U}_h] \\ [P_h] \end{bmatrix} = \begin{bmatrix} -\mathbf{D}^K \\ \mathbf{E}^K \end{bmatrix} [\hat{P}] + \begin{bmatrix} \mathbf{0} \\ \mathbf{F}^K \end{bmatrix}, \tag{8}$$

where $[\mathbf{U}_h]$ and $[P_h]$ denote the degrees of freedom related with the unknowns $\mathbf{U}_h$ and P_h respectively, and the matrices are given by

$$\begin{aligned} A_{ij}^K &:= \int_K \left(\frac{\mathbb{K}}{\mu}\right)^{-1} \boldsymbol{\varphi}_i \cdot \boldsymbol{\varphi}_j, & B_{ij}^K &:= -\int_K \psi_i \, \text{div}\boldsymbol{\varphi}_j, \\ C_{ij}^K &:= \int_e \xi \, \psi_i \, \psi_j, & D_{ij}^K &:= \int_e (\boldsymbol{\varphi}_j \cdot \mathbf{n}) \phi_i, \\ E_{ij}^K &:= \int_e \xi \, \phi_i \, \psi_j, & F_j^K &:= \int_K f \, \psi_j. \end{aligned} \tag{9}$$

Then, we can rewrite the local linear system (8) in a compact form as

$$\begin{bmatrix} \mathbf{M}^K \end{bmatrix} \begin{bmatrix} [\mathbf{U}_h] \\ [P_h] \end{bmatrix} = \begin{bmatrix} -\mathbf{D}^K \\ \mathbf{E}^K \end{bmatrix} [\hat{P}] + \begin{bmatrix} \mathbf{0} \\ \mathbf{F}^K \end{bmatrix}. \tag{10}$$

Imposing the normal trace continuity condition over the edges (6), we obtain the *global lineal system*

$$\sum_{K\in\mathcal{T}_h}\int_{\partial K}(\hat{\mathbf{U}}\cdot\mathbf{n}_K)\phi_j = \sum_{K\in\mathcal{T}_h}\int_{\partial K}\mathbf{U}_h\cdot\mathbf{n}_K - \xi(P_h-\hat{P})\phi_j$$
$$= \begin{bmatrix}\mathbf{D}^K\\ \mathbf{E}^K\end{bmatrix}\begin{bmatrix}[\mathbf{U}_h]\\ [P_h]\end{bmatrix} - \mathbf{R}^K[\hat{P}], \tag{11}$$

where $\mathbf{R}^K$ is a local matrix $R^K_{ij} := \int_e \xi\,\phi_i\,\phi_j$. Replacing (10) in (11) and summing over all $\mathcal{E}_h$:

$$\int_{\mathcal{E}_h}(g_N\,\mathbb{I}_{\mathcal{E}_\Gamma}\cdot\mathbf{n})\phi_j = \sum_{K\in\mathcal{T}_h}\mathbf{X}^K[\hat{P}] + \mathbf{Y}^K,$$

where

$$\mathbf{X}^K = \begin{bmatrix}\mathbf{D}^K\\ \mathbf{E}^K\end{bmatrix}^T \mathbf{M}^{K^{-1}}\begin{bmatrix}-\mathbf{D}^K\\ \mathbf{E}^K\end{bmatrix} - \mathbf{R}^K$$

and

$$\mathbf{Y}^K = \begin{bmatrix}\mathbf{D}^K\\ \mathbf{E}^K\end{bmatrix}^T \mathbf{M}^{K^{-1}}\begin{bmatrix}\mathbf{0}\\ \mathbf{F}^K\end{bmatrix}.$$

Finally, the global system is

$$\mathbf{H}[\hat{P}] = \mathbf{G}_N + \mathbf{K} \tag{12}$$

where $\mathbf{G}_N$ is the null vector except for the positions related to the Newmann boundary. And $\mathbf{H}$ and $\mathbf{K}$ are the assembly of $\mathbf{X}^K$ and $\mathbf{Y}^K$ respectively.

4. Numerical examples

In this section, we will address three examples. We will use the SI units in these equations: $\dot{f}$ in units of volumetric flux, the natural unit of $\mathbb{K}$ is m^2, μ in $\mathrm{Pa}\cdot\mathrm{s}$ and pressure in Pa.

4.1. Laplace equation

Initially we will validate the HDG method with the Laplacian equation in a two dimensional square with Dirichlet boundary condition (Γ_D) except for the north face where the boundary condition is Neumann (Γ_N) as is shown in Figure 2. The flow is assumed to be incompressible, steady-state, Newtonian and the porous medium is isotropic [31]

$$\begin{aligned} -\text{div}\left(\nabla P\right) &= 0 && \text{in } \Omega, \\ -\frac{\partial P}{\partial y} &= \frac{1}{10}\sin\left(\frac{\pi x}{800}\right) && \text{on } \Gamma_N, \\ P &= 0 && \text{on } \Gamma_D. \end{aligned} \tag{13}$$

The analytic solution of the problem (13) is given by

$$P(x,y) = \frac{80}{\pi\cosh(\pi)}\sin\left(\frac{\pi x}{800}\right)\sinh\left(\frac{\pi y}{800}\right). \tag{14}$$

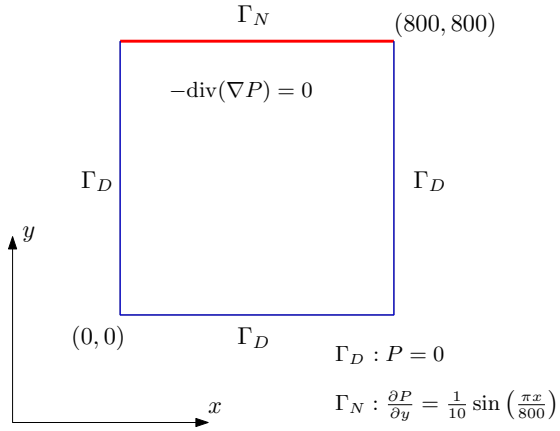

Figure 2: Geometry and boundary conditions of the Laplace equation example.

Figure 3 shows the numerical solution of this problem and the magnitude of the pressure gradient.

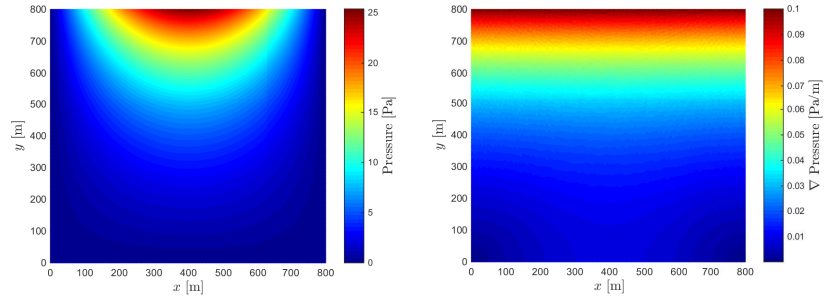

(a) Pressure field. (b) Gradient magnitude.

Figure 3: Numerical solution of the Laplace equation for isotropic case using a mesh with 10784 elements

To analyze the behavior of the flow the streamlined plot is presented in Figure 4. This result indicates that the particles will travel from high to low potentials, being consistent with the equation (2).

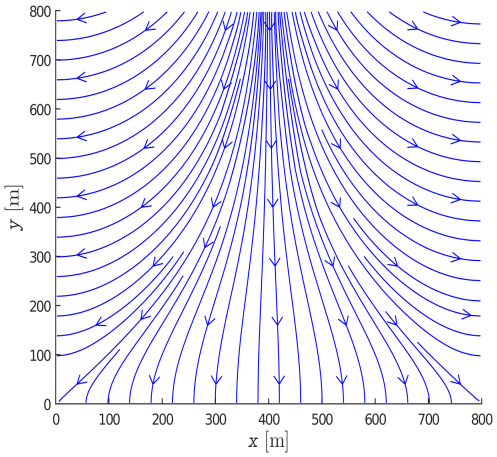

Figure 4: Streamlines of the Laplace example.

The accuracy of the method is computed based on the relative error of the numerical solution using the L^2-norm, i.e $\frac{\|P-P_h\|_2}{\|P\|_2}$.

The convergence of the relative error is presented in Table 1., in terms of the number elements and degrees of freedom (dof) for five different mesh sizes.

nElement	d.o.f	Error
40	360	0.10200
184	1656	0.02016
676	6084	0.00532
2656	23904	0.00129
10784	97056	0.00029

Table 1: Convergence of the error with the L^2-norm.

The error analysis presented in Table 1 indicates that the HDG method is enough accurate and the numerical solution converges to the analytical solution when the mesh is refined.

Now, we will solve the same flow problem in an anisotropic medium with a different permeability tensor

$$\mathbb{K} = \begin{bmatrix} 10^{-10}\,\mathrm{m}^2 & 0 \\ 0 & 1\,\mathrm{m}^2 \end{bmatrix} \tag{15}$$

and viscosity $\mu = 10^{-3}$ Pa $\cdot$ s. The Figure 5 presents the numerical solution of this problem using the HDG method.

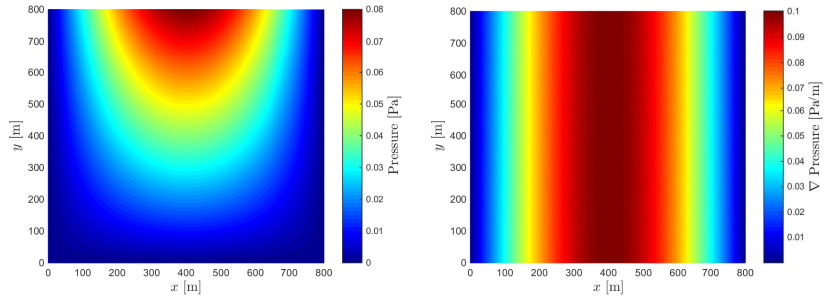

(a) Pressure field. (b) Gradient of the pressure.

Figure 5: Numerical solution of the Laplace equation for the anisotropic case using a mesh with 10784 elements.

Figure 5a shows the pressure field in the anisotropic case, it is sharper than

the isotropic one, although, the boundary conditions are the same in both cases. The source in the top boundary creates a preferential flow through in the y-direction. It is indicated by the high pressure gradient in the central area of Figure 5b. The above mentioned property can be also observed in Figure 6, where the corresponding streamlines coincide with the expected behavior, which is the preferential flow direction [32].

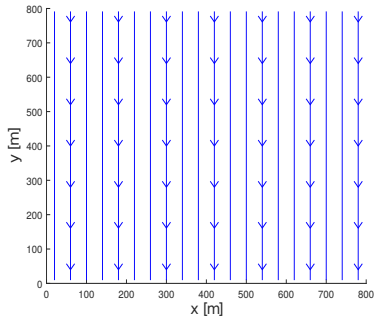

Figure 6: Streamlines of the anisotropic example.

The solution in this example shows the HDG advantage over the traditional unstructured FMV, which has problems of convergence when the ratio between the components of the permeability tensor is larger than 1:1000. [32] That is because the cross diffusion term that appears in cell-centered FVM discretization [12][13] acquires a significant magnitude that affects the global convergence of the method [15][14].

4.2. Five-spots problem

The second problem is a classical two-dimensional flow problem: a confined five-spot pattern where each fluid injector and producer point is assumed to act as a point source and sink (negative source) respectively [33].

4.2.1. Case 1.

The Figure 7, displays the geometry of the five-spot problem domain. Here the single phase flow is assumed incompressible, Newtonian, in steady-state and

the porous medium is isotropic. The analytical solution of this problem is given by:

$$P(x,y) = -\frac{\mu}{4\pi K}\sum_{i=1}^{5} q_i \ln\left((x-x_i)^2 + (y-y_i)^2\right) \tag{16}$$

where $\mu = 10^{-3}$ Pa$\cdot$s, the permeability $K = 10^{-13}$ m^2, and the volumetric flow rate at well i: $\dot{q}_i = \pm 10^{-3}\ \frac{\text{m}^3}{\text{s}}$. In order of the symmetry of this problem, we analyze only one quarter of the problem. Then the injector well and the producer will be at coordinates $(x_1, y_1) = (0, 0)$ and $(x_2, y_2) = (400, 400)$ respectively.

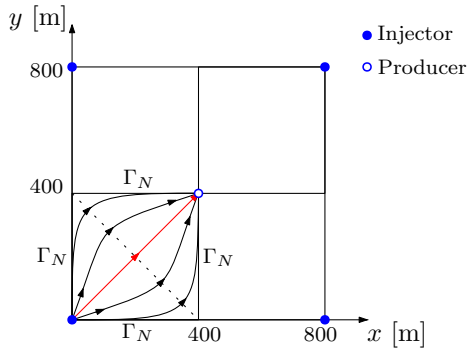

Figure 7: Geometry of the five-spot problem.

Also, since the sources are punctual in the corners, it is necessary to refine the simulation mesh as shown in the Figure 8. This is done in order to reproduce numerically the punctual influence of the source, in the matrix F^k in equation (8).

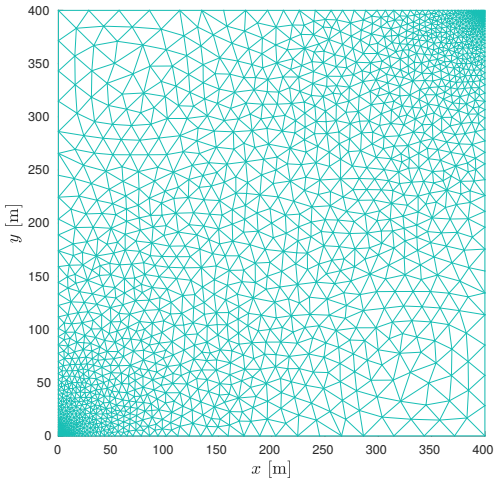

Figure 8: Mesh for the simulation.

The results for this five-spot problem are presented in Figure 9. The pressure field (in MPa) is indicated in the Figure 9a, where a radial variation of the pressure in the neighbor of the wells is observed. Also, Figures 9b and 9c shows the comparative analysis between the analytical solution and the numerical solution along the diagonal of the domain and the y-boundaries respectively. Moreover, the comparison of the volumetric flows at the borders is given in Figure 9d, which are a direct output of the method by directly obtaining the gradients of the solution.

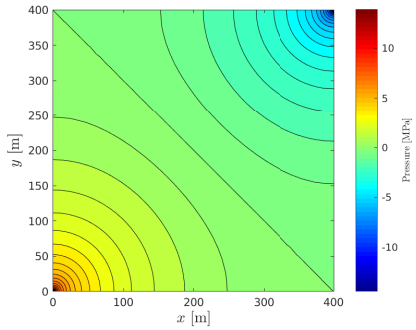

(a) Simulated pressure contours (MPa).

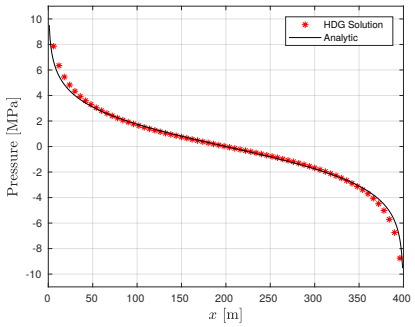

(b) Pressure along the digonal (MPa).

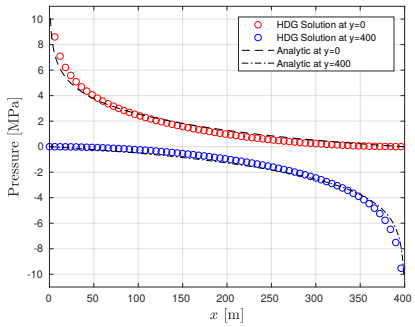

(c) Pressure along the y-boundaries. (MPa).

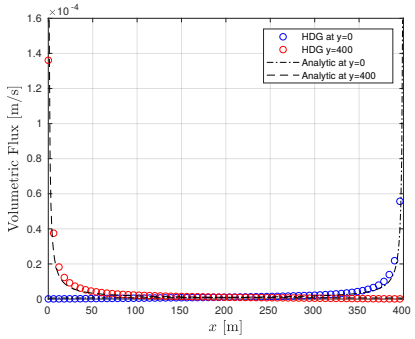

(d) Volumetric flux along the y-boundaries (m/s).

Figure 9: Numerical results of the five-spot problem simulation.

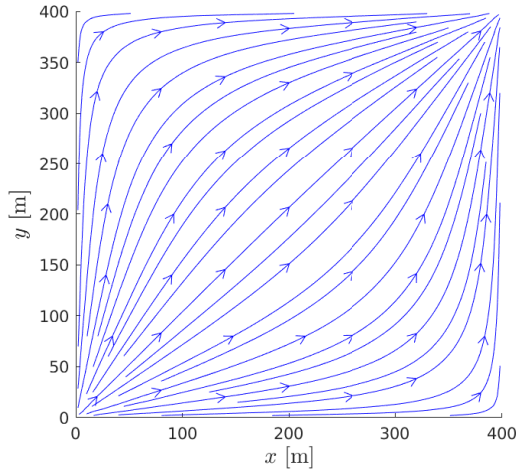

Figure 10: Streamlines of the five spot problem.

The streamlines plot of the five-spot problem is presented in Figure 10. This results indicate that the fluid particles will travel from the injector well to the producer well, through the whole domain.

Finally, the convergence of the relative error is presented in Table 2., in terms of the number elements and degrees of freedom (dof), and mesh size h (maximum element measure), for four different meshes. The error computation is done taking account of the analytical solution presented in equation (16) and using the L^2 norm.

nElement	d.o.f	h [m]	Error
102	918	197.01	0.1632
550	4950	115.04	0.0450
4282	38538	37.75	0.0245
50020	450180	12.19	0.0125

Table 2: Convergence of the error with the L^2-norm.

As it was expected, the error analysis presented in Table 2 indicates that the HDG numerical solution converges to the analytical solution when the mesh is refined.

4.2.2. Case 2.

One of the most important and complex problems in the reservoir simulation is related to the fluid flow in fractured porous media [34]. The classical continuous models of the fractured systems, such as double permeability - double porosity models [35, 36, 37], can not account for the fracture geometry and its interaction with other fractures in the reservoir. A discrete representation of the fracture network systems permits the study of such variables in a reservoir. However, more complexity to the computational grid is added because of the number of elements increases as well as the media heterogeneity. In this case, the traditional methods must be adapted to search heterogeneity interfaces and in most cases, treat the interface as an internal boundary condition [38].

Due to the discontinuous nature of the approximation functions $(\mathbf{U}_h, P_h)$ of HDG formulation, no additional search is required for heterogeneity boundaries, it is enough to set different values of the permeability function $\mathbb{K}(x, y)$ at the neighbor elements in heterogeneity interfaces. Now, to test the versatility of the method, in this case, we will create a highly heterogeneous domain by placing a ultra-low permeability barrier in the center of the domain having a permeability tensor magnitude much lower than the one of flow domain as was done in [33]. Therefore, in this problem, we face a permeability that is not continuous in space. The physical domain of this problem is displayed in the Figure 11.

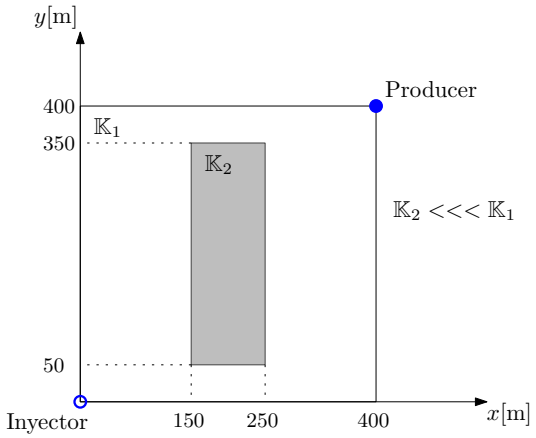

Figure 11: Five-spot problem domain having a low-permeability barrier in the center.

Note that the permeability inside the barrier is not set to zero like in [33], in order not to impose a discontinuous solution of an algorithmic type in the method, *i.e.* modify the implementation to set the trivial solution to the equation (11). In addition, this condition allows distribution of pressures inside the barrier, maintaining the continuity of the field of pressures throughout the domain. This is particularly useful in various fields of application such as, for example, reservoir geomechanics, where it is important to study the deformations of the porous medium due to the stresses produced by fluid flow.

For this case, we consider the same units and flow features that we used in the previous examples, but having the following permeabilities for the domain and the barrier respectively:

$$\mathbb{K}_1 = \begin{bmatrix} 10^{-6}\,\mathrm{m}^2 & 0 \\ 0 & 10^{-6}\,\mathrm{m}^2 \end{bmatrix} \quad \text{and} \quad \mathbb{K}_2 = \begin{bmatrix} 10^{-16}\,\mathrm{m}^2 & 0 \\ 0 & 10^{-16}\,\mathrm{m}^2 \end{bmatrix}. \tag{17}$$

The numerical solution is presented in the Figures 12 and 13.

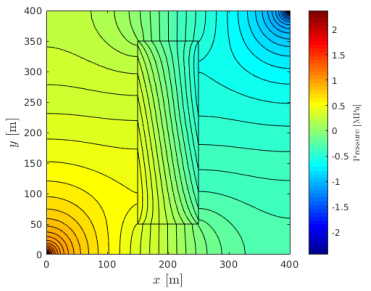

(a) Simulated pressure contours (MPa).

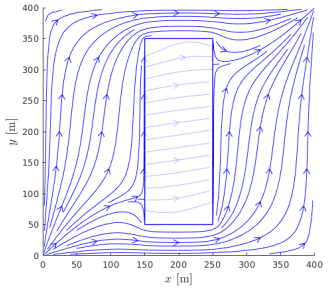

(b) Streamlines of the numerical solution.

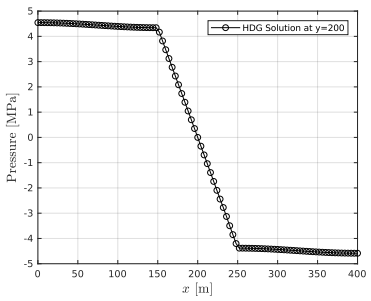

(c) Contour of the numerical solution pressure.

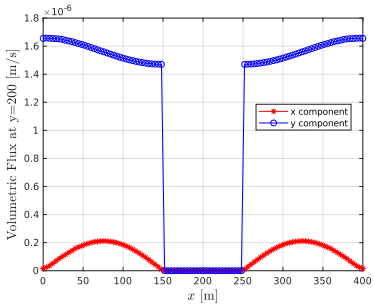

(d) Volumetric flux components at $y = 200$ (m/s).

Figure 12: Numerical solution in the heterogeneous case with 43136 elements.

One important result is that, despite the pressure field it is continuous (Figure 12a), the discontinuous permeability tensor field creates a discontinuous velocity filed, as observed at the interface of the barrier in the Figure 12d. Flow will proceed through preferential areas (high permeability zones) as the streamlines indicate in the Figure 12b. Additionally, the Figure 13 shows the magnitude of the gradient obtained directly as a result of the method. In this figure is evident the discontinuous nature of the HDG method, element by element, particularly in the jump of the velocity solution due to the abrupt change of the material in the faces of the barrier.

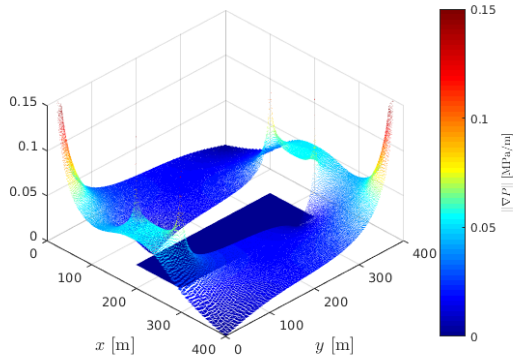

Figure 13: Pressure gradient magnitude for the five-spot problem in heterogeneous case (MPa/m).

By the Darcy equation and the equation (2), there is a proportionality relationship between the magnitude of the pressure gradient and the magnitude of the flow velocity in the porous media. Note also that, except for the regions around the source and the sink, there is an increase in the gradient in the narrow zones between the barrier and the north and south boundaries, indicating a significant increase in velocity that coincides with the narrowing of the streamlines in the Figure 12b. Also, it is important to note that, due to the very low permeability in the barrier, the flow velocity is almost zero in the portion of the domain occupied by that obstacle.

5. Conclusion

This work is the basis for the construction of more robust numerical methods to face major problems related to flow in highly anisotropic and heterogeneous porous media, as many applications in the oil industry. It seems convenient to use numerical methods based on variational formulations of porous media because this approach allows more efficient modeling of flow dynamics in media with very special characteristics as a naturally fractured media. In highly anisotropic media, the HDG method proves to be efficient and this gives an idea about other applications that can have taking advantage over the classic

methods as FVM and FEM.

As we show in the five spot problem with the barrier, HDG method takes advantage of the discontinuous nature of the solution, and his gradient (see Figure 13), in heterogeneous porous media where the permeability function is highly discontinuous in space. This property of the mixed methods is particularly useful to calculate the velocity fields of the solution in this kind of heterogeneous domains because the proportionality relation between the gradient and the velocity given by Darcy's law. Also, is important to note that the proposed HDG formulation can simulate such discontinuities without any extra assumption or additional computational expense as searching algorithms usually required for heterogeneity interfaces. Additionally, HDG has a fundamental advantage over the classical DG methods, which is the reduction of the degrees of freedom in the formulation, because the normal trace continuity weakly imposed in the solution. In addition, HDG for the mixed formulation possesses conservative properties, like FVM, with the inherited advantages of the finite element method.

The next stage of this work is to analyze and to compare the performance of the HDG method here presented with respect to the classical methods as FVM and FEM. The current development and implementation of HDG are planned to be extended to more general diffusion problems involving time, three-dimensional domains and two face flow.

Acknowledgments

Authors thank Equion, COLCIENCIAS and the Agencia Nacional de Hidorcarburos for financial support under Contract No. 647-2015: *eWAG - Uso de nanotecnoligía para el potenciamiento de la técnica de recobro mejorado de agua alternada con gas (WAG)*. Authors also thank the Universidad Nacional de Colombia for logistic and financial support.

References

[1] H. Hoteit, A. Firoozabadi, Multicomponent fluid flow by discontinuous Galerkin and mixed methods in unfractured and fractured media, Water Resources Research 41 (11) (2005) W11412. doi:10.1029/2005WR004339. URL http://onlinelibrary.wiley.com/doi/10.1029/2005WR004339/abstract

[2] S. P. Neuman, Saturated-unsaturated seepage by finite elements., in: J. HYDRAUL. DIV., PROC., ASCE., 1973.

[3] P. R. Johnson, N. Sun, M. Elimelech, Colloid transport in geochemically heterogeneous porous media: Modeling and measurements, Environmental science & technology 30 (11) (1996) 3284–3293.

[4] T. Xu, J. Samper, C. Ayora, M. Manzano, E. Custodio, Modeling of non-isothermal multi-component reactive transport in field scale porous media flow systems, Journal of Hydrology 214 (1) (1999) 144 – 164. doi:https://doi.org/10.1016/S0022-1694(98)00283-2. URL http://www.sciencedirect.com/science/article/pii/S0022169498002832

[5] T. N. Narasimhan, P. A. Witherspoon, An integrated finite difference method for analyzing fluid flow in porous media, Water Resources Research 12 (1) (1976) 57–64. doi:10.1029/WR012i001p00057. URL http://dx.doi.org/10.1029/WR012i001p00057

[6] M. R. Islam, M. E. Hossain, S. H. Mousavizadegan, S. Mustafiz, J. H. Abou-Kassem, Advanced Petroleum Reservoir Simulation: Towards Developing Reservoir Emulators, John Wiley & Sons, 2016.

[7] Y. Achdou, C. Bernardi, F. Coquel, A priori and a posteriori analysis of finite volume discretizations of darcy's equations, Numerische Mathematik 96 (1) (2003) 17–42. doi:10.1007/s00211-002-0436-7. URL https://doi.org/10.1007/s00211-002-0436-7

[8] L. C. Young, A Finite-Element Method for Reservoir Simulation, Society of Petroleum Engineers Journal 21 (01) (1981) 115–128. doi:10.2118/7413-PA.
URL https://www.onepetro.org/journal-paper/SPE-7413-PA

[9] O. C. Zienkiewicz, T. Shiomi, Dynamic behaviour of saturated porous media; the generalized biot formulation and its numerical solution, International Journal for Numerical and Analytical Methods in Geomechanics 8 (1) (1984) 71–96. doi:10.1002/nag.1610080106.
URL http://dx.doi.org/10.1002/nag.1610080106

[10] A. Masud, T. J. Hughes, A stabilized mixed finite element method for darcy flow, Computer Methods in Applied Mechanics and Engineering 191 (39) (2002) 4341 – 4370. doi:https://doi.org/10.1016/S0045-7825(02)00371-7.
URL http://www.sciencedirect.com/science/article/pii/S0045782502003717

[11] S. Ye, Y. Xue, C. Xie, Application of the multiscale finite element method to flow in heterogeneous porous media, Water Resources Research 40 (9) (2004) n/a–n/a, w09202. doi:10.1029/2003WR002914.
URL http://dx.doi.org/10.1029/2003WR002914

[12] H. Jasak, Error analysis and estimation for finite volume method with applications to fluid flow.

[13] F. Juretic, Error analysis in finite volume cfd, Ph.D. thesis, Imperial College London (University of London) (2005).

[14] D. Loudyi, R. A. Falconer, B. Lin, Mathematical development and verification of a non-orthogonal finite volume model for groundwater flow applications, Advances in water resources 30 (1) (2007) 29–42.

[15] J. Pasdunkorale A, I. W. Turner, A second order finite volume technique

for simulating transport in anisotropic media, International Journal of Numerical Methods for Heat & Fluid Flow 13 (1) (2003) 31–56.

[16] E. Sozer, C. Brehm, C. C. Kiris, Gradient calculation methods on arbitrary polyhedral unstructured meshes for cell-centered cfd solvers, in: Proceedings of the 52nd Aerospace Sciences Meeting, National Harbor, MD, USA, Vol. 1317, 2014.

[17] I. Turner, W. Ferguson, An unstructured mesh cell-centered control volume method for simulating heat and mass transfer in porous media: Application to softwood drying, part i: The isotropic model, Applied Mathematical Modelling 19 (11) (1995) 654 – 667. doi:https://doi.org/10.1016/0307-904X(95)00087-Z.
URL http://www.sciencedirect.com/science/article/pii/0307904X9500087Z

[18] V. Dalen, Simplified Finite-Element Models for Reservoir Flow Problems, Society of Petroleum Engineers Journal 19 (05) (1979) 333–343. doi:10.2118/7196-PA.
URL https://www.onepetro.org/journal-paper/SPE-7196-PA

[19] C. L. McMichael, G. W. Thomas, Reservoir Simulation by Galerkin's Method, Society of Petroleum Engineers Journal 13 (03) (1973) 125–138. doi:10.2118/3558-PA.
URL https://www.onepetro.org/journal-paper/SPE-3558-PA

[20] R. E. Ewing, The Mathematics of Reservoir Simulation, SIAM, 1983.

[21] M. Ainsworth, A synthesis of a posteriori error estimation techniques for conforming, non-conforming and discontinuous galerkin finite element methods, Contemporary Mathematics 383 (2005) 1–14.

[22] P. Hansbo, M. G. Larson, Discontinuous galerkin and the crouzeix–raviart element: application to elasticity, ESAIM: Mathematical Modelling and Numerical Analysis 37 (1) (2003) 63–72.

[23] B. Cockburn, G. E. Karniadakis, C.-W. Shu, The Development of Discontinuous Galerkin Methods, in: B. Cockburn, G. E. Karniadakis, C.-W. Shu (Eds.), Discontinuous Galerkin Methods, no. 11 in Lecture Notes in Computational Science and Engineering, Springer Berlin Heidelberg, 2000, pp. 3–50, dOI: 10.1007/978-3-642-59721-3_1.
URL http://link.springer.com/chapter/10.1007/978-3-642-59721-3_1

[24] N. C. Nguyen, J. Peraire, B. Cockburn, Hybridizable discontinuous galerkin methods, in: Spectral and High Order Methods for Partial Differential Equations, Springer, 2011, pp. 63–84.

[25] B. Cockburn, J. Gopalakrishnan, R. Lazarov, Unified Hybridization of Discontinuous Galerkin, Mixed, and Continuous Galerkin Methods for Second Order Elliptic Problems, SIAM Journal on Numerical Analysis 47 (2) (2009) 1319–1365. doi:10.1137/070706616.
URL http://epubs.siam.org/doi/abs/10.1137/070706616

[26] B. Cockburn, J. Guzmán, H. Wang, Superconvergent discontinuous galerkin methods for second-order elliptic problems, Mathematics of Computation 78 (265) (2009) 1–24.

[27] B. Cockburn, J. Shen, A hybridizable discontinuous galerkin method for the p-laplacian, SIAM Journal on Scientific Computing 38 (1) (2016) A545–A566. arXiv:https://doi.org/10.1137/15M1008014, doi:10.1137/15M1008014.
URL https://doi.org/10.1137/15M1008014

[28] A. Loula, M. Correa, J. Guerreiro, E. Toledo, On finite element methods for heterogeneous elliptic problems, International Journal of Solids and Structures 45 (25) (2008) 6436 – 6450. doi:https://doi.org/10.1016/j.ijsolstr.2008.08.005.
URL http://www.sciencedirect.com/science/article/pii/S0020768308003296

[29] G. N. Gatica, A simple introduction to the mixed finite element method, Theory and Applications. Springer Briefs in Mathematics. Springer, London.

[30] B. Cockburn, J. Gopalakrishnan, F.-J. Sayas, A projection-based error analysis of hdg methods, Mathematics of Computation 79 (271) (2010) 1351–1367.

[31] E. A. Lynd, J. T. Foster, Q. P. Nguyen, et al., An application of the isogeometric analysis method to reservoir simulation, in: SPE Europec featured at 78th EAGE Conference and Exhibition, Society of Petroleum Engineers, 2016.

[32] W. Ferguson, I. Turner, A control volume finite element numerical simulation of the drying of spruce, Journal of Computational Physics 125 (1) (1996) 59 – 70. doi:https://doi.org/10.1006/jcph.1996.0079.
URL http://www.sciencedirect.com/science/article/pii/S0021999196900790

[33] A. Katiyar, J. T. Foster, H. Ouchi, M. M. Sharma, A peridynamic formulation of pressure driven convective fluid transport in porous media, Journal of Computational Physics 261 (Supplement C) (2014) 209 – 229. doi:https://doi.org/10.1016/j.jcp.2013.12.039.
URL http://www.sciencedirect.com/science/article/pii/S0021999113008474

[34] M. Sahimi, Flow and transport in porous media and fractured rock: from classical methods to modern approaches, John Wiley & Sons, 2011.

[35] H. R. Ghafouri, R. W. Lewis, A finite element double porosity model for heterogeneous deformable porous media, International Journal for Numerical and Analytical Methods in Geomechanics 20 (11) (1996) 831–844. doi:10.1002/(SICI)1096-9853(199611)20:11<831::AID-NAG850>3.0.CO;2-6.

URL http://dx.doi.org/10.1002/(SICI)1096-9853(199611)20:11<831::AID-NAG850>3.0.CO;2-6

[36] R. W. Lewis, H. R. Ghafouri, A novel finite element double porosity model for multiphase flow through deformable fractured porous media, International Journal for Numerical and Analytical Methods in Geomechanics 21 (11) (1997) 789–816. doi:10.1002/(SICI)1096-9853(199711)21:11<789::AID-NAG901>3.0.CO;2-C.
URL http://dx.doi.org/10.1002/(SICI)1096-9853(199711)21:11<789::AID-NAG901>3.0.CO;2-C

[37] P. S. Huyakorn, B. H. Lester, J. W. Mercer, An efficient finite element technique for modeling transport in fractured porous media: 1. single species transport, Water Resources Research 19 (3) (1983) 841–854. doi:10.1029/WR019i003p00841.
URL http://dx.doi.org/10.1029/WR019i003p00841

[38] A peridynamic formulation for transient heat conduction in bodies with evolving discontinuities, Journal of Computational Physics 231 (7).